JOURNAL OF GEOPHYSICAL RESEARCH, VOL. 112, XXXXXX, doi:10.1029/2007JA012348, 2007

Oxygen ions at Titan's exobase in a Voyager 1–type interaction from a hybrid simulation

I. Sillanpää,[1] E. Kallio,[1] R. Jarvinen,[1] and P. Janhunen[1]

Received 15 February 2007; revised 10 May 2007; accepted 25 September 2007; published XX Month 2007.

[1] Titan's extensive atmosphere and exosphere interact with Saturn's rotating magnetospheric flow. We have studied this interaction with an advanced hybrid simulation model which employs a realistic ion composition in the upstream flow (subsonic $O^+$and H^+) and has improved spatial resolution. We present results for both the general characteristics of the interaction and the behavior of the O^+flow ions near the exobase for the conditions during the Voyager 1 flyby. Our model shows that the ionotail and the magnetotail bend in a direction opposite to the convection electric field. This is validated with the total force on the incident flow species derived from basic plasma equations. We also present a simulated impact map for the oxygen ions of the flow with total O^+precipitation rate 1.3×10^{24} s^{-1} at Titan's exobase. Although this rate indicates that the plasma conditions above the exobase do not inhibit O^+precipitation on the exobase, the direction of the O^+flow is shown to turn drastically near the exobase. The energy deposition of the medium-weight flow ions (such as O^+) thus seems to be orders of magnitude larger than the energy deposition by pickup ions formed near Titan. However, the lightweight flow ions (H^+) are effectively deflected by the magnetic barrier formed around Titan.

Citation: Sillanpää, I., E. Kallio, R. Jarvinen, and P. Janhunen (2007), Oxygen ions at Titan's exobase in a Voyager 1–type interaction from a hybrid simulation, *J. Geophys. Res., 112*, XXXXXX, doi:10.1029/2007JA012348.

1. Introduction

[2] Titan, the second largest planetary satellite of the solar system, orbits Saturn in the outer Kronian magnetosphere. Titan's nitrogen-rich atmosphere is very substantial with hydrocarbon clouds and hazes extending up to 500 km above its surface [*Porco et al.*, 2005]. Titan's exosphere consisting mainly of N_2, CH_4, and H_2 molecules and neutral hydrogen atoms [*Waite et al.*, 2005; *Niemann et al.*, 2005; *Coustenis*, 1994] is also very extensive owing to low gravity. There are various physical processes taking place at and above the height above which there are only negligible collisions with neutral particles. For Titan this height, the exobase, was measured to be about 1430 km during Cassini's first close flyby TA [*Waite et al.*, 2005]. Important processes above the exobase include magnetic draping, ionization of the neutral exosphere and subsequent ion pickup.

[3] The Voyager 1 flyby of Titan in November 1980 gave the first in situ measurements of the magnetic field and plasma quantities around Titan [*Hartle et al.*, 1982; *Ness et al.*, 1982; *Neubauer et al.*, 1984]. The snapshot it provided was rather incomplete. Our view of Titan has partly changed and very much sharpened with the Cassini mission to the Kronian system. In particular, the particle composition in the nearly corotating magnetospheric plasma [*Young et al.*, 2005; *Szego et al.*, 2005] as well as in Titan's ionosphere [*Waite et al.*, 2005; *Cravens et al.*, 2004] is now much more accurately known. This places new challenges also for modelers to provide new understanding for the observed details with a self-consistent, three-dimensional picture of Titan's plasma interaction. While the data set by Cassini is far from complete at the moment owing to the highly variable plasma environment at Titan's orbit, there are, however, many new details being published continually as Cassini's mission progresses. Two recent articles on measurements during Cassini's Titan flybys are by *Hartle et al.* [2006] and *Neubauer et al.* [2006]. Hartle et al. discuss the ion and electron measurements obtained with Cassini/CAPS instruments during flyby TA that compare well with the measurements with the plasma science instrument onboard Voyager 1. Neubauer et al. focus on the magnetic fields measured during Cassini's first three close flybys at Titan and compare them with results from an MHD simulation model.

[4] This work presents results from our hybrid simulation model developed for Titan's magnetospheric interaction, and here we have taken a special focus on the characteristics of the interaction near the exobase. Among the new results is a O^+precipitation map at Titan's exobase. We discuss the behavior of different ion populations especially near the exobase and their effect on the general features of the interaction. Even though our model does not include sputtering effects and neutral collisions at the moment, it

[1]Finnish Meteorological Institute, Helsinki, Finland.

0148-0227/07/2007JA012348$09.00

takes into account self-consistently the effects of asymmetric ion motion and corresponding magnetic field behavior.

[5] Earlier studies pertinent to our current study are other hybrid and MHD simulation studies on Titan's magnetospheric interaction. Generally the MHD simulations are good at modeling the ion production through different ionization processes and taking into account various chemical reactions. The advantage of hybrid simulations is that they can model the behavior of various ion species independently and take that behavior into account self-consistently in the field propagation. Numerous three-dimensional or global simulation results have been published for Titan during the last decade [e.g., *Simon et al.*, 2006; *Ma et al.*, 2006; *Nagy et al.*, 2001; *Brecht et al.*, 2000; *Kabin et al.*, 1999, 2000; *Ledvina and Cravens*, 1998]. Among the recent results from these simulations are the following. *Simon et al.* [2006] used their hybrid code to show the different behavior of pickup ions according to their masses in Titan's ionospheric tail, as suggested by *Luhmann* [1996]. *Ma et al.* [2006] made comparisons to plasma and magnetic field measurements from Cassini's first Titan flybys using their MHD simulation model with a sophisticated chemical scheme for the ionosphere's composition. Also Monte Carlo simulations have been made to estimate impact rates and the energy deposition on Titan's exobase using MHD simulation results [*Michael and Johnson*, 2005; *Michael et al.*, 2005; *Ledvina et al.*, 2005; W.-L. Tseng et al., Exospheric heating by pickup ions at Titan, submitted to *Advances in Space Research*, 2006, hereinafter referred to as Tseng et al., submitted manuscript, 2006], but the restriction of these studies has been that the ion motion is not taken into account self-consistently in the magnetic and electric fields used. One interesting result by *Michael and Johnson* [2005] is that ions of both magnetospheric and exospheric origin deposit more total energy in Titan's upper atmosphere than the solar radiation. This result clearly underlines the importance of studying the spacial distribution of the ion impacts on Titan's exobase.

[6] The ion precipitation into an atmosphere gives rise to various physical phenomena as the precipitating ions have elastic and inelastic collisions with neutral atoms and molecules of the atmosphere. In collisional reactions ions can ionize neutrals and thus be a source of new electrons and ions. The resulting electrons increase the conductivity and can therefore affect the electric currents and also the magnetic fields at lower altitudes. The new ions, on the other hand, can interact with the neutrals resulting in new ion species. Some reactions result in excited neutrals that emit photons as they return to the ground state. The elastic collisions are a source of neutral heating. However, a quantitative estimation of these effects call for more extensive studies, for example three-dimensional (3-D) Monte Carlo (MC) simulations. There is a plausible and already applied scenario of using the impact rates from a hybrid model in such studies. As a first step, the ion impact rates are derived with a hybrid model, then the rates of various elastic and inelastic collisions are calculated with a three-dimensional MC model, and finally the obtained rates are used as source terms in a photochemical model. These steps were taken with Mars studies a few years ago [see *Kallio and Janhunen*, 2001; *Kallio and Barabash*, 2001; *Haider et al.*, 2002].

[7] We give a brief description of the model and the parameters used in this study in the next section. In the results section we present a general description of the interaction from our simulation results as well as some key quantities at Titan's exobase, e.g., the radial flow of O^+. We then discuss the implications of the results and compare them with other studies. Finally a brief summary is given.

2. Simulation Model

[8] We used a global hybrid simulation model developed at the Finnish Meteorological Institute and recently revised (the new version includes hybrid models for Titan, Venus and Mars). We chose to use Voyager 1 type conditions for the interaction as the Voyager 1 flyby provides a good nominal case.

[9] Our model for Titan employed 5 ion species: $H^+$and O^+ ions for the rotating magnetospheric flow and N_2^+, CH_4^+ and H_2^+ for the pickup ions. The flow parameters for upstream were as follows: The upstream number densities were 0.1 and 0.2 cm^{-3} for H^+ and O^+, respectively, while the bulk velocity 120 km/s and the Maxwellian thermal velocity v_{th} = 180 km/s were the same for both ($T_{H+} = 3.9 \times 10^6$ *K*, $T_{O+} = 6.2 \times 10^7$ *K*, and $v_{th} = \sqrt{k_B T/m}$). The upstream magnetic field was 5.0 nT. This means that the sound speed was v_S = 220 km/s (= $\sqrt{\gamma}\, v_{th}$ with γ = 3/2) and the Alfvén speed 60 km/s. Thus the magnetospheric plasma flow was subsonic and super-Alfvénic. We used somewhat smaller thermal velocities than those detected by Voyager 1 (*Neubauer et al.* [1984]; see also *Sittler et al.* [2005]), but otherwise the parameters were the same.

[10] The right-handed coordinate system is as follows. With the origin at the center of Titan, the X axis points against the direction of the magnetospheric rotational plasma flow and the upstream magnetic field is 5 nT in the $-$Z direction. Thus the convection electric field $\vec{E}_C = -\vec{U}_e \times \vec{B}$ is in +Y direction and has the value 0.6 mV/m in the upstream. If we assume Z to be northward normal to the orbital plane and the flow direction along Titan's orbit, then $-$Y points to Saturn; this we call the nominal orientation.

[11] Total emission rates for the ions produced at Titan were as follows: For H_2^+ and CH_4^+ ions a Chamberlain neutral ionization profile was used with density and temperature values from *Garnier et al.* [2007]. They used INMS data from Cassini's early flybys to update the exospheric profiles. We discretized the neutral density function to simulation cells, and with ionization rate of 2.0×10^{-9} s^{-1} for solar radiation (the sunlit area of the exosphere) this yielded a production rate 8.5×10^{24} s^{-1} for H_2^+. The production rate for methane ions CH_4^+ was calculated in a similar way with a solar ionization rate 2.0×10^{-8} s^{-1} and yielded a production rate 3.3×10^{24} s^{-1} for CH_4^+. We used solar ionization rates provided by *Huebner et al.* [1992] and chose to use the higher values given for active Sun conditions. The optical shadow, where no production of methane and molecular hydrogen ions took place, was for Saturn local time (SLT) 13.5 h as per the Voyager 1 flyby. Nitrogen molecular ions N_2^+ were produced with a rate of 5.0×10^{24} s^{-1} uniformly at the exobase (r = 4125 km, distance from the center of Titan) with a small velocity ($\sim$2 km/s) away from Titan. Results with this production rate compared better with Cassini/MAG data from the T9

flyby (P. Garnier, unpublished data, 2004) than results with the larger value 1.6×10^{25} s^{-1} we used earlier [*Sillanpää et al.*, 2006]. The production of N_2^+ ions directly at the exobase is justified as the density-scale height is very small compared to the cell size of the simulation grid.

[12] The simulation box had a base cell size of 0.4 R_T (= 1030 km, R_T = 2575 km) with boundaries for each of the coordinates: X from -11.2 R_T to 8.8 R_T, Y from -11.2 R_T to 11.2 R_T, and Z from -8.8 R_T to 8.8 R_T. We used a denser grid closer to Titan with cell size half the base cell size (0.2 R_T = 515 km) for the following area: -9.2 R_T < X < 5.2 R_T, -7.6 R_T < Y < 7.6 R_T, -5.2 R_T < Z <, 5.2 R_T. We used absorbing boundary conditions at r = 3500 km while the electron velocity was set to zero below r = 3800 km preventing the fields from penetrating any deeper into ionosphere as if by a very high conductivity in the ionosphere. The outer boundary conditions were very close to those described in our earlier paper [*Sillanpää et al.*, 2006].

[13] We use two methods for determining the impact rates on the exobase for the ions of the incoming flow. One is the absorption rate that we obtain by counting all the absorptions at the inner absorbing boundary. The other method uses average density and velocity values in grid cells for the selected ion species. We interpolate these grid values to points on the exobase r = 4200 km. The interpolated values were calculated in three spatial dimensions from weighted corner values of the cells in which the interpolation points were located. The corner values were in turn an average of the values in the adjacent cells. The local flux through the exobase is the product of the interpolated values of the number density and the radial velocity. The total impact rate is the sum of products of these fluxes and the corresponding exobase surface areas. This we call the derived impact rate. These methods can in principle be used also for the exospheric ions, but their production in our hybrid model is not self-consistent at the exobase.

[14] The fields and particles were propagated using the following formulas during each time step in a leapfrog scheme (which is not explicitly written here). First each particle is moved by a displacement

$$d\vec{x}_i = \vec{v}_i dt, \tag{1}$$

where index i labels each macroparticle and dt is the time step. The second step is the propagation of the electromagnetic fields. This starts with the calculation of the electric current density $\vec{j}$ as a curl of the magnetic field $\vec{B}$:

$$\vec{j} = \mu_0^{-1} \nabla \times \vec{B}. \tag{2}$$

[15] Then the electron velocity U_e is calculated from another formula for the current density:

$$\vec{j} = q_e n_e \vec{U}_e + \sum_k q_k n_k \vec{v}_k, \tag{3}$$

where we use the quasi-neutrality:

$$n_e = \sum_k q_k n_k / |q_e|. \tag{4}$$

n_k and q_k are the number density and the electric charge for each ion species k and q_e is the electron charge. Now the electric field can be obtained from the Ohm's law:

$$\vec{E} = -\vec{U}_e \times \vec{B} + \vec{j}/\sigma. \tag{5}$$

[16] The change in the magnetic field B is then calculated with Faraday's law of induction:

$$d\vec{B} = -dt \, \nabla \times \vec{E}. \tag{6}$$

[17] Finally, with the fields updated we can propagate the velocity of each macroparticle with the Lorentz force equation:

$$d\vec{v}_i = q_i \left(\vec{E} + \vec{v}_i \times \vec{B}\right) dt / m_i. \tag{7}$$

[18] For efficiency, macroparticles representing ion species may be joined with other particles representing the same ion species or split into two macroparticles. This splitting and joining of the macroparticles is done during each time step and in each grid cell with a probability that increases as the number of macroparticles differs from a target number. The target number for macroparticles per cell was 50 in this simulation, and thus the total number of macroparticles in the box at any given moment of the simulation run was around 18 million. Further numerical details of our model are given in a paper by *Kallio and Janhunen* [2001] and upon request. The simulation run reached a quasi-steady state with an ionotail developed in about 2500 s and the results presented in this article are from around 2800 s.

3. Results

[19] We present the key results from the simulation run to provide both a general view of the interaction as well as a view of the area around the exobase. The overall picture of the interaction remains much the same as in our previous results (cf. *Sillanpää et al.* [2006] and especially the SLT 12-h case; see also the subsonic case by *Kallio et al.* [2004]).

3.1. Magnetic Field Near Titan

[20] Figure 1 shows the total magnetic field in two planes along the upstream flow direction. In the Y = 0 plane parallel to ambient magnetic field (Figure 1a), we see that the magnetic tail lobes extend over 5 R_T from the middle of the wake in a direction that is parallel to the ambient magnetic field. The current sheet between the lobes is seen as a straight band with a total magnetic field less than 3 nT extending from Titan in the direction opposite to the incoming flow. In the Z = 0 plane parallel to the convection electric field $\vec{E}_C$ (Figure 1b) it is seen that the magnetotail bends in the direction opposite to $\vec{E}_C$ (or toward Saturn in the nominal orientation) and extends from Y = -3 to 1 R_T. One can also notice that the current sheet, seen as an area of low magnetic field, is quite extended in the Y direction. Some artifacts are present where the grid density changes around X = -8.5 R_T. The maximum of the magnetic field is located more on the +Y hemisphere of Titan rather than in

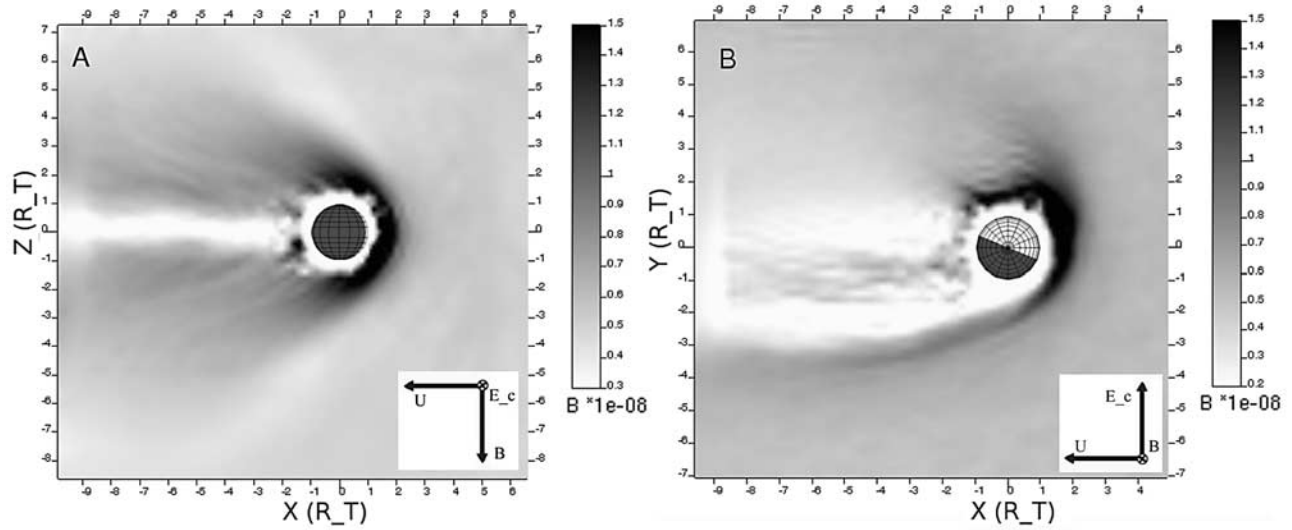

Figure 1. Total magnetic field in the (a) Y = 0 and (b) Z = 0 planes. The grayscale shows 3–15 and 2–15 nT, respectively, with the high end (in black) saturated.

the center of the ramside, as was seen clearly also in our previous study [*Sillanpää et al.*, 2006].

[21] The draping of the magnetic field lines is shown in Figure 2. The magnetic tail lobes are clearly seen in Figure 2a. The current sheet between the lobes is not as sharp as expected; this is due to our finite cell size that is rather large compared to the width of the current sheet. The asymmetry of the interaction can also be seen in the draping pattern (see Figure 2b); there seems to be one draping layer on the ramside of the magnetic barrier and another below it. In Figure 3 we show the magnitude and direction of the magnetic field at the height of the exobase. The magnetic field is very symmetric in the north-south direction, as expected from the symmetry of the situation. However, the magnetic field is much larger in the sector between the ram direction and the +Y direction (aligned with $\vec{E}_C$) than in any other direction. The vector plot (Figure 3b) shows how well-formed the magnetic lobe structure is down to the exobase especially on the −Y side; on the northern hemisphere the magnetic field points against the incoming flow while on the southern hemisphere the field direction is opposite. Directly against the flow the direction of the magnetic field of the exobase is unchanged from the upstream direction; also the field direction is along the exobase surface on the ramside but the radial component increases toward the wakeside.

3.2. Ions Near Titan

[22] The total ion density from the simulation is shown in Figure 4 in the same Y = 0 and Z = 0 planes as for the total magnetic field in Figure 1. In Figure 4a, there

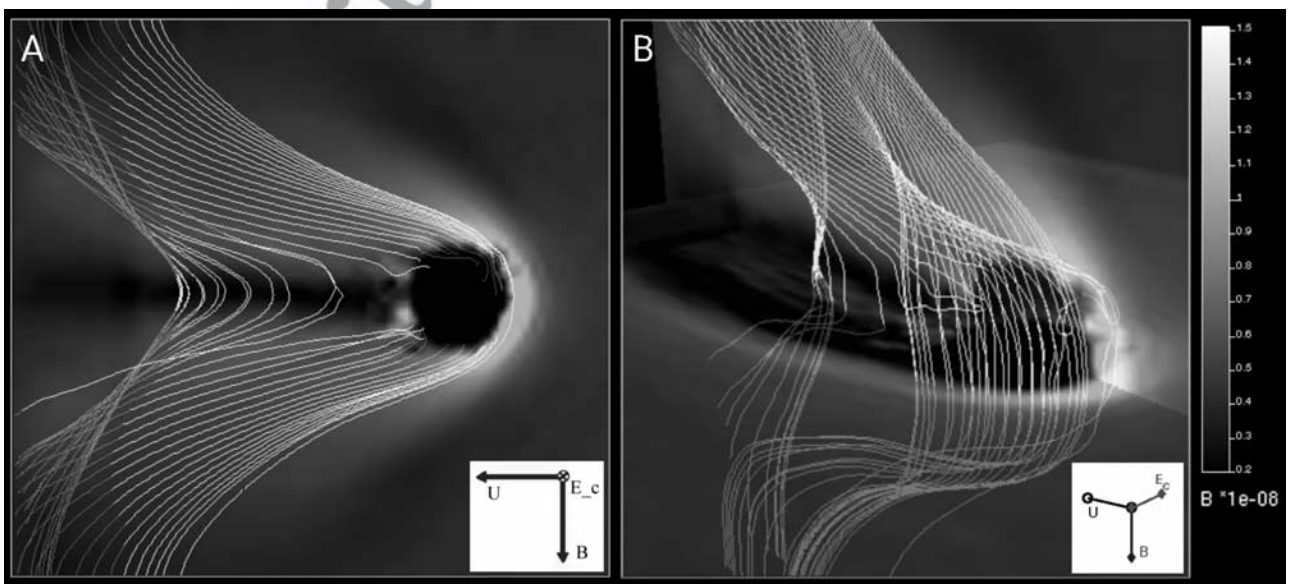

Figure 2. Magnetic field lines around Titan. The grayscale on the planes drawn (Y = 0 and Z = 0) shows the total magnetic field 2–15 nT in both panels. The field lines were drawn from lines parallel to the Z axis in the wake. (a) X = −7.5 R_T, Y = 0 R_T, Z = −6.5 to 6.5 R_T. (b) X = −5 R_T, Y = −0.5 R_T, Z = 0 to 7 R_T.

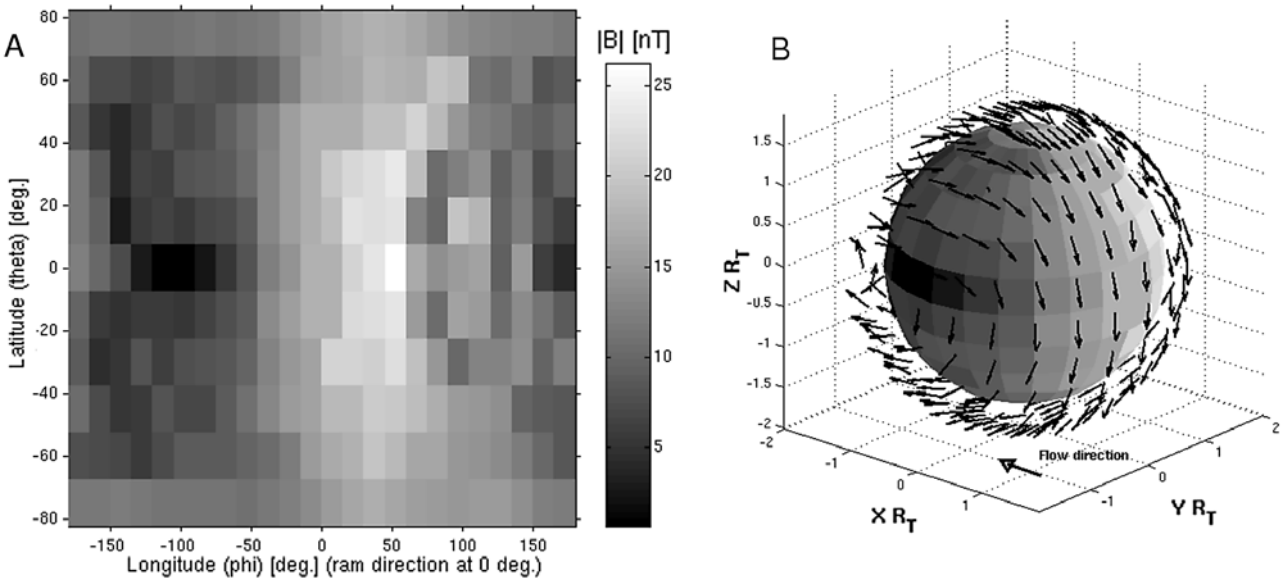

Figure 3. (a) Total magnetic field at r = 4200 km plotted as a two-dimensional map. (b) Unit vectors of the magnetic field at the same height. Vectors are drawn above the surface for clarity. The grayscale 1–26 nT is the same in Figures 3a and 3b. The direction of the flow is indicated with an arrow. In Figure 3a the horizontal axis corresponds to the angle phi, which is defined with zero in the direction of X axis (against the undisturbed flow) and increasing toward the +Y direction; zero longitude in the plots is in the ram direction. The vertical axis is the angle theta, which corresponds to the latitude in the nominal orientation with zero in the equator and increasing northward.

are areas of low ion density coaligning with the front sides of the magnetic tail lobes (cf. Figure 1). In these areas the convection electric field $\vec{E}_C = -\vec{U}_e \times \vec{B}$ is close to the upstream value owing to large $\vec{B}$ even though the electron velocity $\vec{U}_e$ is decreasing with the bulk ion flow. Therefore the newly ionized particles here are quickly picked up by the flow. The main feature in Figure 4b is the bent ionotail with high concentration of ions (dominated by N_2^+ and CH_4^+). In the nominal orientation the bending is toward Saturn.

[23] The ion density is high all around Titan within $r < 2\,R_T$ and thus the exosphere close to Titan acts as a diamagnetic obstacle for the magnetic field carried by the incoming flow. (There are white areas within the absorption radius in all the

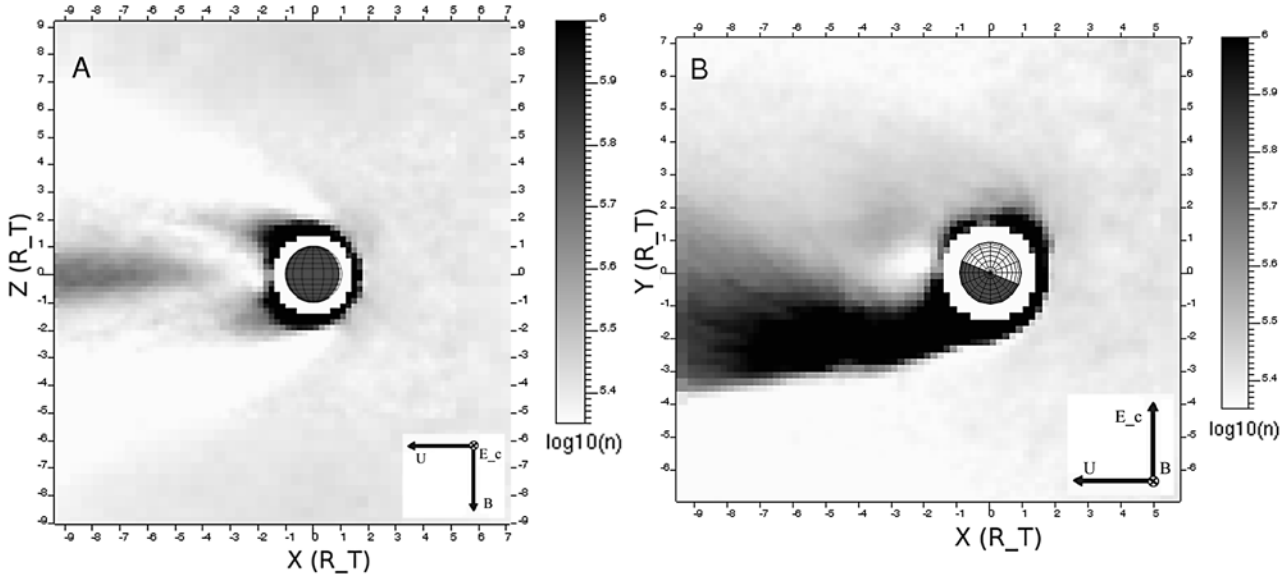

Figure 4. Total ion number density, including H^+ and O^+ ions for the rotating magnetospheric flow and N_2^+, CH_4^+, and H_2^+ for the emitted ions in the (a) Y = 0 and (b) Z = 0 planes. The color values are logarithmic ($\log_{10}[m^{-3}]$) with range limits equal to 0.20 cm^{-3} and 1.0 cm^{-3} in Figures 4a and 4b.

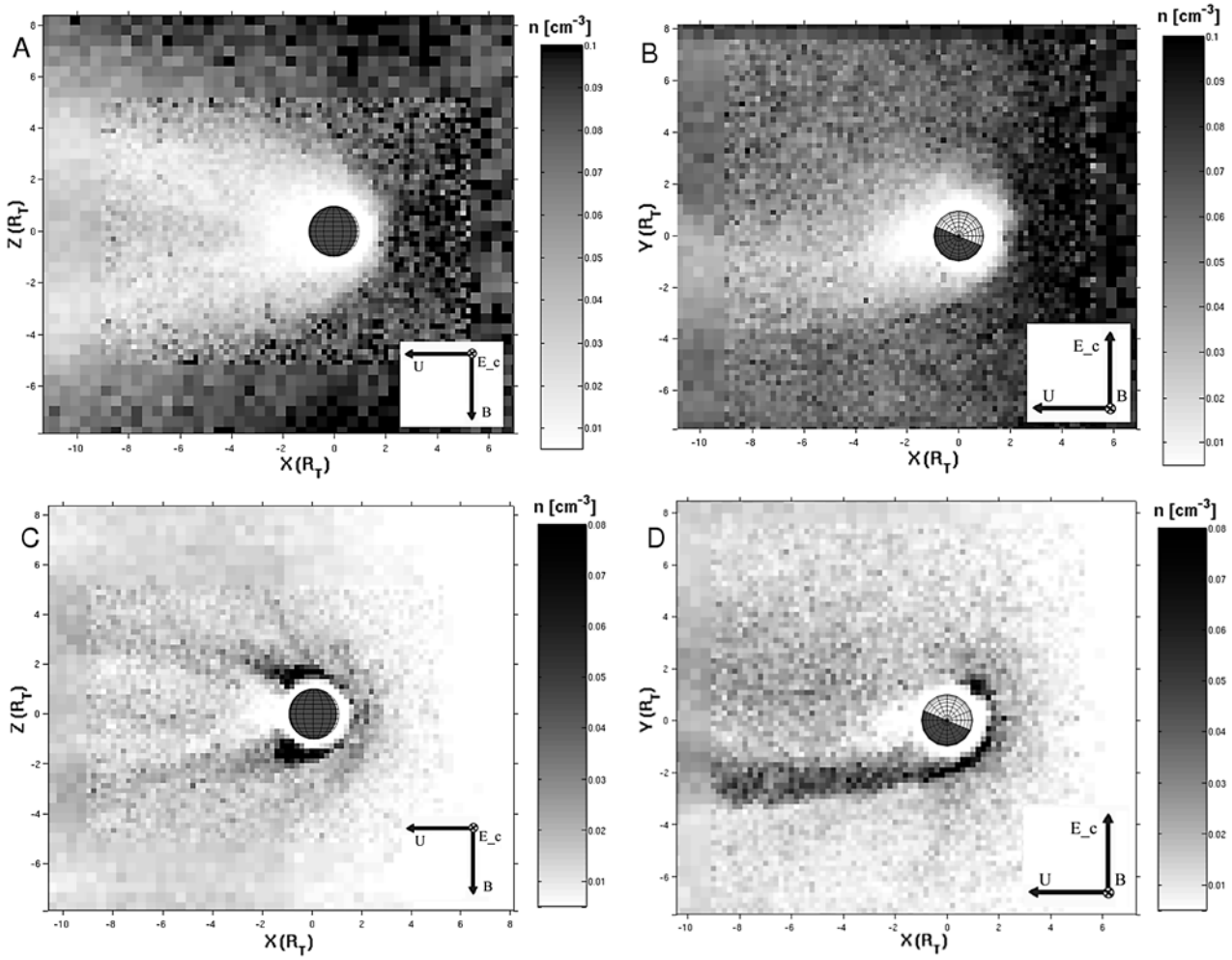

Figure 5. (a and b) Number density of H^+ ions of the rotating flow and (c and d) H_2^+ ions of the exosphere. Figures 5a and 5c plot the Y = 0 plane, while Figures 5b and 5d plot the Z = 0 plane. For H^+ the colorscale is 0.005–0.1 cm^{-3} and for H_2^+ 0.005–0.08 cm^{-3}.

density plots.) In Figure 4a, there are areas of enhanced ion density starting from near the Z axis (X −2 to 0 R_T, Z ± 2 R_T) and extending tailward and along the draped magnetic field lines (cf. Figure 2a). Though the total magnetic field is large here at the bases of the magnetic tail lobes, the convection electric field nearly vanishes as the bulk velocity and the draping magnetic field are almost parallel there. Thus the ions created from neutrals by ionization can collect here as the convection electric field exerts a very small force on them. These extensions of high ion density emerge from what could be the ionospheric foot points for wings of Alfvén waves. The Alfvén wings would have existed at Titan during the Voyager 1 flyby according to *Kivelson* [2004]. Some minor features can be seen in Figure 4. There is a small area of low ion density located very close to Titan at X = −2 R_T in the middle of the wake. Also in Figure 4a there are emerging ions in the middle of the wake after X = −3 R_T. These are ions from the bent tail being accelerated in the +Y direction by the convection electric field.

[24] H^+ and H_2^+ densities from the simulation are shown in Figure 5 for the Y = 0 and Z = 0 planes. H^+ ions of the incoming flow cannot penetrate the areas with a strong magnetic field, although O^+ ions are almost uninhibited owing to their much larger mass and gyroradius. (O^+ densities are not shown here as the only feature discernible is a density decrease in a very small area in Titan's immediate wake.) The protons are effectively shielded away owing to their small gyroradius (in undisturbed upstream conditions only 250 km). Molecular hydrogen ions H_2^+ are created by ionization from Titan's broad cloud of neutral molecular hydrogen. The density plots for H_2^+ show the same main characteristics found in total ion density plots (Figure 4).

3.3. Impacting O^+ Ions

[25] We studied also the behavior of O^+ ions of the incoming flow at Titan's exobase using our simulation results. Figure 6 shows the direction of the velocity and the density of O^+ ions at the exobase. In Figure 6a the O^+ flow is turned in −Y direction on the ramside and also on the +Y side of Titan's exobase. On the −Y side the velocity is along the surface of the exobase. These two trends meet in the antiram meridian where the velocities are again toward Titan's interior. In the density map (Figure 6b) the number density of O^+ ions is quite symmetric with respect to the ram direction where the highest densities are

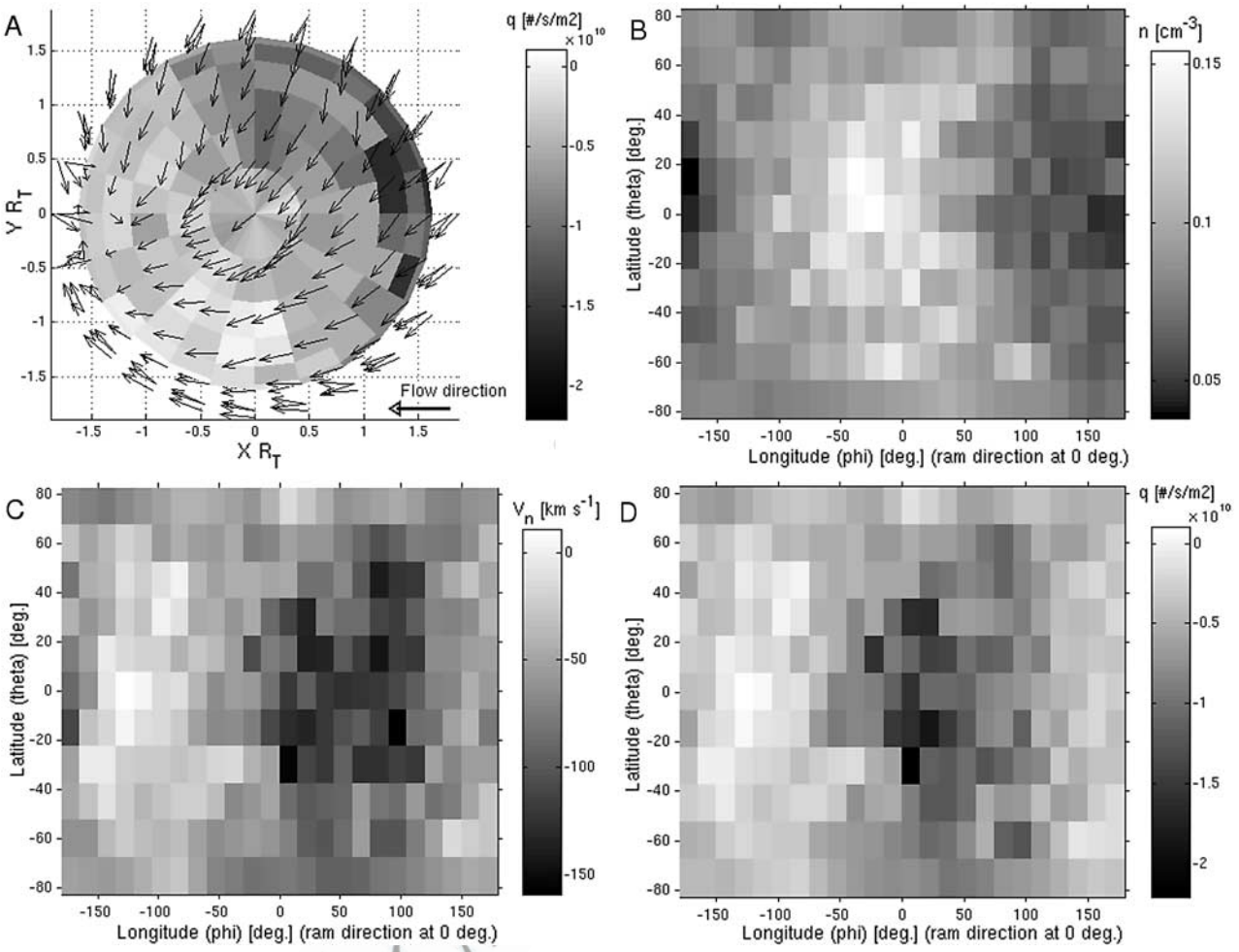

Figure 6. Flow of atomic oxygen ions O^+ at Titan's exobase. (a) O^+ velocity unit vectors projected onto a X − Y plane at $r = 4200$ km are shown. The view point of this three-dimensional plot is above the Z = 0 plane (i.e., the orbital plane in the nominal orientation). The surface in this panel shows the derived O^+ flux through the surface (see Figure 6d). The unit vectors are drawn a little above the surface for clarity. (b) The O^+ density at $r = 4200$ km is shown. Phi and theta in Figures 6b–6d are defined as in Figure 3. (c) The radial velocity (v_N, positive away from Titan) map for O^+ is shown. (d) The flux of O^+ through the exobase surface is shown. The flux was derived as $q = v_N \times n$. Summing the negative values (toward Titan) of the flux map and weighting them with the corresponding surface area yields a total impact rate 1.34×10^{24} s^{-1} for O^+ ions.

found. The radial velocity map in Figure 6c shows a large area of higher velocities toward Titan on the +Y side of Titan. Both of these 2-D maps of the exobase were created with the 3-D interpolation method described in the model section.

[26] In Figure 6d is the O^+ flux map at $r = 4200$ km. It is a product of the values in O^+ density and radial velocity maps in Figure 6b and 6c, respectively. The maximum derived impact rate per area was over 20,000 O^+ ions/s/cm^2, which value corresponds the flux in the undisturbed upstream flow with the parameters used. The total impact rate derived from this flux map is 1.34×10^{24} s^{-1} for O^+ ions. This value seems reasonably reliable as the absorption rate of O^+ at the inner absorption boundary was $1.3–1.4 \times 10^{24}$ s^{-1}. The absorption rate for H^+ was as a low as 1.1×10^{23} s^{-1} even though the density of protons was twice the density of O^+ ions in the upstream flow.

[27] An estimate of the energy deposition of O^+ ions on the exobase can be obtained by assuming that the average impact energy can be calculated locally from the average radial velocities (here the assumption is a beam-like distribution):

$$E_{prec} = \int_S q \times m_O + v_N^2 \, dS, \tag{8}$$

where the integration is over the surface of the exobase, q is the flux of O^+ ions at the exobase in units $m^{-2}s^{-1}$, and m_{O+} and v_N are the mass and the average radial velocity of the O^+ ions, respectively. For our discretized flux map of the exobase this gives 310 MW as the total energy deposition rate on the exobase by impacting O^+. However, the precipitation energy of the flow protons from our simulation

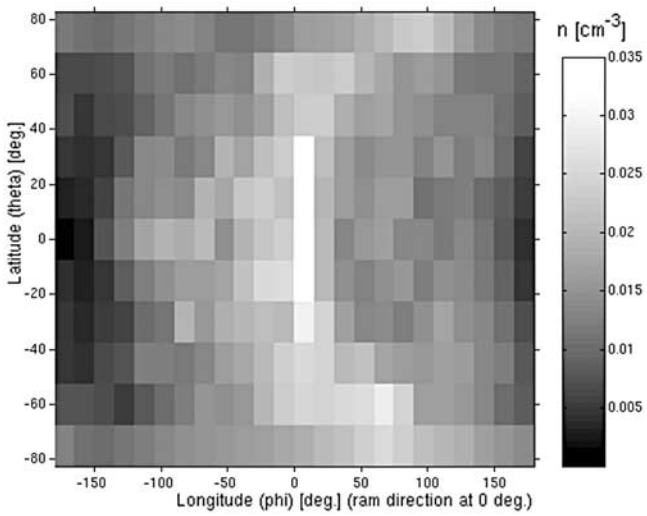

Figure 7. The H^+ density map at $r = 4200$ km is shown. See Figure 3 for an explanation of the axes. The grayscale is $0-0.035$ cm^{-3} with the high end saturated. The maximum value was 0.045 cm^{-3}.

is only 2 to 3 MW with impact rate 1×10^{23} s^{-1} on the exobase.

[28] The proton density at the exobase is shown in Figure 7. The radial velocity of H^+shows much fluctuation at the exobase and is not presented. When Figure 7 is compared with the total magnetic field and the density of O^+ at the exobase (Figures 2 and 6), the main features seem very similar. In all these mappings the highest values are located near the zero latitude. The areas of high values extend northward and southward from the equator in an angle so that the highest values at ±60 to ±80 degrees of latitude have a shift around +90 degrees in the phi coordinate from the equatorial maximum. These features seem to occur in the same location for both of the flow ion species with the equatorial maximum at phi equal to −40 to 0 degrees. The total magnetic field maximum is located more on the +Y side with the equatorial maximum at phi equal to +20 to +60 degrees.

[29] We have made simulation runs also with larger CH_4^+ and N_2^+ production rates (+75% and +40%, respectively, with a similar Chamberlain density profile) than those in the simulation run presented. The general characteristics remained very much the same, and change in the derived impact rates of the flow ions was less than 10%. Thus we feel confident that the O^+ precipitation is quite stable with respect to the production rates of the pickup ions.

4. Discussion

[30] The results presented in this paper give a global view of the effects that the motion of ions has on Titan's magnetospheric plasma interaction when taken into account self-consistently. The greatest differences to the results from MHD models are the asymmetries in the plane perpendicular to the upstream magnetic field (e.g., Z = 0). Namely, the bending of the tail structures in the direction of $-\vec{E}_C$ and the shift of the maximum magnetic field from the ram direction. Both of these results on the asymmetries of the interaction are in agreement with our previous study [*Sillanpää et al.*, 2006]. The acceleration of pickup ions in the direction of the convection electric field $\vec{E}_C$ causes an opposite force on the incoming flow of ions as can be seen in the following analysis.

[31] Using equations (3), (4), and (5) we can rewrite the average Lorentz force in the hybrid scheme on an ion of species i using the bulk velocity of that ion species $\vec{U}_i$. Multiplying the result with the number density n_i gives the local force density accelerating the ion species i:

$$n_i m_i \frac{d\vec{U}_i}{dt} = n_i q_i \left(\vec{E} + \vec{U}i \times \vec{B}\right) = n_i q_i \left(\sigma^{-1}\vec{j} + \frac{\vec{j} \times \vec{B}}{\sum_k n_k q_k}\right) + n_i q_i \frac{\sum_{k \neq i} n_k q_k \left(\vec{U}_i - \vec{U}_k\right)}{\sum_k n_k q_k} \times \vec{B} \tag{9}$$

[32] One can notice that the latter term, which is proportional to differences between the bulk velocities of the ion species, vanishes when both sides of the equation are summed over all ion species. Thus the average force on all the ions is only $\vec{j} \times \vec{B}$ and the resistivity term. In Hall-MHD simulations the force on individual ions is exactly that. However, the latter term in equation (9) is crucial when considering the bulk motion of the individual species and it has been used qualitatively in analysis of the solar wind mass loading near Mars and comets [cf. *Kallio and Janhunen*, 2001, section 3.4.2; *Omidi and Winske*, 1987, section 3]. The difference between the average force on the pickup ions and the incident flow can be determined by dividing the simulation particles roughly into two classes: pickup ions near Titan with negligible initial velocities (class 1) and ions of the incident flow (class 2) with bulk velocity $\vec{U}_2$ in the −X direction. On the pickup ions the force is in the direction of $-\vec{U}_2 \times \vec{B}$, where $\vec{B}$ is in the −Z direction. Thus the total force on the newly generated pickup ions (class 1) is in the +Y direction, i.e., in the direction of the convection electric field $\vec{E}_C = -\vec{U}_e \times \vec{B}$. On the ions of the incident flow (class 2) the force is in the opposite direction. This seems to explain the behavior of the incident O^+ ions in Figure 6a.

[33] The turning of the upstream flow gives a reason for the bending of the tail structure toward Saturn in the nominal orientation. In addition, the stagnation point of the incoming plasma flow is located near the maximum of magnetic field in the magnetic barrier, i.e., on the +Y side of Titan's ram direction. Thus the above analysis explains the main asymmetries found in the interaction. Other plausible causes for asymmetries, namely gradient and curvature drifts, are very local and cannot explain the turning of the O^+ flow even in locations where these drifts would be the strongest (i.e., where the gradients and the curvature of the magnetic field are large). The finite gyromotion of ions in itself plays a role in the asymmetries through absorption into Titan's ionosphere, but it would not be important in the wake.

[34] Other features in our results besides the stated asymmetries include the strong magnetic lobes in the wake

and the narrow current sheet between the lobes. Our results seem to be in accordance with *Neubauer et al.* [2006] who found near the equatorial plane of the draping coordinates what the call the polary reversal layer with thicknesses of 320 km and 230 km for TA and T3 flybys, respectively. Furthermore, our results show relatively high ion densities in the magnetic tail lobes near Titan and low ion density elsewhere in the lobes where the magnetic field strength was large. Moreover, the mass of the pickup ions did not seem to play a role in their migration nor in the main features of the ion density. This is seen in the way even the lightest ionized species used, H_2^+, showed the same main features as seen in the total ion density that was dominated by the heavier species, namely the bent ionotail and density enhancements in the magnetic tail lobes near Titan. All in all, the broad area where H_2^+ ions are created seems to form only a weak and seemingly negligible obstacle for the ion flow.

[35] In this study the incident flow consisted of protons and O^+ ions with their thermal velocities exceeding the bulk velocity. Their ability to penetrate through the magnetic barrier and into the magnetic lobes was very different; while the proton density drops by a factor of ten within the lobes, there cannot be seen any decrease in the O^+ density. Also the O^+ impacts on the exobase seems to be nearly uninhibited by the magnetic barrier as the O^+ densities and velocities at the exobase can even exceed the upstream averages. On the other hand the H^+ was to a large degree deflected by the magnetic barrier. The determining factor for the trajectory of an ion and especially its ability to penetrate Titan's magnetic barrier is its magnetic rigidity:

$$R_{mag} = mv_\perp/q = r_L B, \qquad (10)$$

where m is the mass of the ion, $v_\perp$ is its speed perpendicular to the magnetic field and q its charge, r_L is its Larmor radius and B the magnetic field strength. At this point we can only make a rough estimate for a cutoff magnetic rigidity that would determine the minimum rigidity necessary for an upstream ion to penetrate through Titan's magnetic barrier. This limit for the magnetic rigidity would be of the order of 1 $R_T \times 5$ nT in Voyager 1–like conditions, on the basis of the magnetic rigidities of $H^+$and O^+ions as their average upstream gyroradii are 0.097 R_T and 1.6 R_T, respectively, and the upstream magnetic field strength is 5 nT.

[36] We have made a preliminary run with thermal velocities 240 km/s for protons and O^+, corresponding to the reported thermal velocities during the Voyager 1 flyby [*Neubauer et al.*, 1984], and with the same upstream densities; the derived impact rate on the exobase was $1.55–1.6 \times 10^{24}$ s^{-1}, for O^+ and for protons the rate was $1.3–1.4 \times 10^{23}$ s^{-1}. Thus for both species the precipitation increased about 20%. There are, however, some questions whether such high thermal velocities would be common at Titan's orbit.

[37] Other studies most relevant to this work are by Tseng et al. (submitted manuscript, 2006) and *Ledvina et al.* [2005]. Both groups made Monte Carlo simulations on ion precipitation on Titan's exobase using MHD simulation results for the electromagnetic fields around Titan. This means that the fields they employed were not consistent with the asymmetries owing to ion drifts and other effects of finite gyroradii. Their values for the precipitation rates of pickup ions are consistent with each other [cf. Tseng et al., submitted manuscript, 2006, Table 1] and provide a good reference point for our study. Tseng et al. studied the three most prominent pickup ion species at Titan with different local times along Titan's orbit. Their case of Saturn local time 12 h is closest to the Voyager 1 case that we used. Their total energy precipitation rate of all three pickup species is 2.4 MW that is two orders of magnitude less than the O^+ energy deposition rate on the exobase in our simulation. *Ledvina et al.* [2005] studied the impact rates of the pickup ions like Tseng et al. but also the impact rates of the flow species. They state that the precipitation of N^+ ions (their medium-weight flow species with a Maxwellian velocity distribution) on the exobase was nearly unhindered with a precipitation rate 1.7×10^{24} that is close to our value for O^+. Their value for the precipitation of the flow protons (also Maxwellian) was 3.9×10^{22} s^{-1}, which is less than half of ours. This difference in the proton precipitation is probably partly due to the unrealistically symmetric magnetic field used by Ledvina et al. in their study; however their spatial resolution was better than ours as the cell size of their model was between 164 and 230 km near the exobase.

[38] Our simulation shows that the densities of the flow species (H^+ and O^+) are several orders of magnitude lower than the total ion density at Titan's exobase, where the ion density is dominated by the exospheric ions. Models by *Cravens et al.* [2004] and *Keller et al.* [1992] give for the electron density at the exobase values around 300 cm^{-3}. This confirms that the direct contribution of the flow ions to the total ion density is negligible at this height, even though their energy deposition is large.

[39] Currently the Cassini spacecraft has made several Titan flybys with the closest approach below the exobase. This kind of flyby makes it possible to study also the precipitating magnetospheric ions as they would be detectable at the exobase by their high velocity among the much more abundant thermal ions. The Cassini Plasma Spectrometer (CAPS) [*Young et al.*, 2004] onboard Cassini would be an appropriate instrument for detecting these magnetospheric ions, but as with particle instruments in general its measurements are highly dependent on the orientation of the spacecraft. It is possible that a suitable data set already exists to perform such a study.

[40] In this study we focused on the behavior of the upstream ions near Titan. This is partly because there are quite a few more parameters, physical and related to numerics, in the ionization process near Titan than with the upstream flow: the photoionization depends on the solar EUV flux [*Floyd et al.*, 2002; *Bossy*, 1983] and direction, ionization cross sections, exobase height, and on the neutral profile that in turn depends on the mass, temperature and density of the neutral particle species at the exobase. Furthermore, the photoionization depends on the method the whole process is numerically handled in the computer simulation. One important open aspect concerns the roles that the now neglected effects of impact ionization and electron pressure (and possibly even gravity) can have in the behavior and interactions of Titan's ambient plasma.

[41] Our next Titan study will be based on increasing the spatial resolution of the ion precipitation maps. This will be done by collecting directly the macroparticle velocities and locations at the exobase. This way not only the flux maps can be accurately formed but also maps of the energy deposition. Increasing the resolution of the simulation grid near Titan will be another important development of our simulation model for Titan. That might allow us to make accurate estimates for the cutoff magnetic rigidity for the magnetic barrier and find the fine structure in the magnetic tail lobes or possibly Venus-like tail ray filaments (see *Luhmann et al.* [1991] for general Titan-Venus comparison or *Luhmann* [1993] and *Brace and Kliore* [1991] for Venus tail ray studies).

5. Summary

[42] We have studied ion behavior at Titan's exobase using a hybrid simulation code with self-consistent ion and field propagation. Our results continue to demonstrate the strong asymmetry in the tail region of Titan with respect to the direction of the convection electric field. The precipitation rates of the flow ions (O^+ and H^+) agree with the earlier results by *Ledvina et al.* [2005]. The clearly dominant energy import to Titan's exobase is by the medium-weight ions in the Kronian rotating plasma flow whose precipitation is not inhibited by the magnetic barrier, even though the flow of oxygen ions is shown to turn almost to the direction opposite to the convection electric field on the ramside and the anti-Saturn side of Titan in the nominal orientation. We show that this turning of the incident flow can be derived from the equations of the hybrid scheme. We have also presented a map of O^+ precipitation on Titan's exobase, which is a novel result. The rate of the total energy precipitation by particles is of the order of hundreds of MW and is most likely nearly directly proportional to the upstream flux of medium-weight ions.

[43] **Acknowledgments.** Wolfgang Baumjohann thanks Thomas Cravens and another reviewer for their assistance in evaluating this paper.

References

Bossy, L. (1983), Solar indices and solar UV-irradiances, *Planet. Space*, *31*, doi:10.1016/0032-0633(83)90089-2.

Brace, L. H., and A. J. Kliore (1991), The structure of the Venus ionosphere, *Space Sci. Rev.*, *55*, 81–163.

Brecht, S. H., J. G. Luhmann, and D. J. Larson (2000), Simulation of the Saturnian magnetospheric interaction with Titan, *J. Geophys. Res.*, *105*, 13,119–13,130.

Coustenis, A. (1994), Titan's atmosphere and surface: Parallels and differences with the primitive Earth, *Earth Moon Planets*, *67*, 95–100.

Cravens, T. E., J. Vann, J. Clark, J. Yu, C. N. Keller, and C. Brull (2004), The ionosphere of Titan: An updated theoretical model, *Adv. Space Res.*, *33*, 212–215.

Floyd, L., W. K. Tobiska, and R. P. Cebula (2002), Solar UV irradiance, its variation, and its relevance to the Earth, *Adv. Space Res.*, *29*, 1427–1440.

Garnier, P., I. Dandouras, D. Toublanc, P. C. Brandt, E. C. Roelof, D. G. Mitchell, S. M. Krimigis, N. Krupp, D. C. Hamilton, and H. Waite (2007), The exosphere of Titan and its interaction with the Kronian magnetosphere: MIMI observations and modeling, *Planet. Space Sci.*, *55*, 165–173, doi:10.1016/j.pss.2006.07.006.

Haider, S. A., S. P. Seth, E. Kallio, and K. I. Oyama (2002), Solar EUV and electron-proton-hydrogen atom-produced ionosphere on Mars: Comparative studies of particle fluxes and ion production rates due to different processes, *Icarus*, *159*(1), 18–30, doi:10.1006/icar.2002.6919.

Hartle, R. E., E. C. Sittler Jr., K. W. Ogilvie, J. D. Scudder, A. J. Lazarus, and S. K. Atreya (1982), Titan's ion exosphere observed from Voyager 1, *J. Geophys. Res.*, *87*, 1383–1394.

Hartle, R. E., et al. (2006), Initial interpretation of Titan plasma interaction as observed by the Cassini plasma spectrometer: Comparisons with Voyager 1, *Planet. Space Sci.*, *54*, doi:10.1016/j.pss.2006.05.029.

Huebner, W. F., J. J. Keady, and S. P. Lyon (1992), Solar photo rates for planetary atmospheres and atmospheric pollutants, *Astrophys. Space Sci.*, *195*, 1–294.

Kabin, K., T. I. Gombosi, D. L. DeZeeuw, K. G. Powell, and P. L. Israelevich (1999), Interaction of the Saturnian magnetosphere with Titan: Results of a three-dimensional MHD simulation, *J. Geophys. Res.*, *104*, 2451–2458.

Kabin, K., P. L. Israelevich, A. I. Ershkovich, F. M. Neubauer, T. I. Gombosi, D. L. DeZeeuw, and K. G. Powell (2000), Titan's magnetic wake: Atmospheric or magnetospheric interaction, *J. Geophys. Res.*, *105*, 10,761–10,770.

Kallio, E., and S. Barabash (2001), Atmospheric effects of precipitating energetic hydrogen atoms on the Martian atmosphere, *J. Geophys. Res.*, *106*(A1), 165,178.

Kallio, E., and P. Janhunen (2001), Atmospheric effects of proton precipitation in the Martian atmosphere and its connection to the Mars-solar wind interaction, *J. Geophys. Res.*, *106*, 5617–5634.

Kallio, E., I. Sillanpää, and P. Janhunen (2004), Titan in subsonic and supersonic flow, *Geophys. Res. Lett.*, *31*, L15703, doi:10.1029/2004GL020344.

Keller, C. N., T. E. Cravens, and L. Gan (1992), A model of the ionosphere of Titan, *J. Geophys. Res.*, *97*, 12,117–12,135.

Kivelson, M. G. (2004), Moon-magnetosphere interactions: A tutorial, *Adv. Space Res.*, *33*, 2061–2077.

Ledvina, S. A., and T. E. Cravens (1998), A single fluid three-dimensional MHD model of plasma flow around Titan, *Planet. Space Sci.*, *46*, 1175–1191.

Ledvina, S. A., T. E. Cravens, and K. Kecskemty (2005), Ion distributions in Saturn's magnetosphere near Titan, *J. Geophys. Res.*, *110*, A06211, doi:10.1029/2004JA010771.

Luhmann, J. G. (1993), A model of the ionospheric tail rays of Venus, *J. Geophys. Res.*, *98*, 17,615–17,622.

Luhmann, J. G. (1996), Titan's ion exosphere wake: A natural ion mass spectrometer?, *J. Geophys. Res.*, *101*, 29,387–29,393.

Luhmann, J. G., C. T. Russell, K. Schwingenschuh, and Y. Yeroshenko (1991), A comparison of induced magnetotails of planetary bodies: Venus, Mars, and Titan, *J. Geophys. Res.*, *96*, 11,199–11,208.

Ma, Y., A. F. Nagy, T. E. Cravens, I. V. Sokolov, K. C. Hansen, J.-E. Wahlund, F. J. Crary, A. J. Coates, and M. K. Dougherty (2006), Comparisons between MHD model calculations and observations of Cassini flybys of Titan, *J. Geophys. Res.*, *111*, A05207, doi:10.1029/2005JA011481.

Michael, M., and R. E. Johnson (2005), Energy deposition of pickup ions and heating of Titan's atmosphere, *Planet. Space Sci.*, *53*, 1510–1514, doi:10.1016/j.pss.2005.08.001.

Michael, M., R. E. Johnson, F. Leblanc, M. Liu, J. G. Luhmann, and V. I. Shematovich (2005), Ejection of nitrogen from Titan's atmosphere by magnetospheric ions and pick-up ions, *Icarus*, *175*, 263–267.

Nagy, A. F., Y. Liu, K. C. Hansen, K. Kabin, T. I. Gombosi, M. R. Combi, D. L. DeZeeuw, K. G. Powell, and A. J. Kliore (2001), The interaction between the magnetosphere of Saturn and Titan's ionosphere, *J. Geophys. Res.*, *106*, 6151–6160.

Ness, N. F., M. H. Acuna, and K. W. Behannon (1982), The induced magnetosphere of Titan, *J. Geophys. Res.*, *87*, 1369–1381.

Neubauer, F. M., D. A. Gurnett, J. D. Scudder, and R. E. Hartle (1984), Titan's magnetospheric interaction, in *Saturn*, edited by T. Gehrels and M. S. Matthews, pp. 760–787, Univ. of Ariz. Press, Tucson.

Neubauer, F. M., et al. (2006), Titan's near magnetotail from magnetic field and electron plasma observations and modeling: Cassini flybys TA, TB, and T3, *J. Geophys. Res.*, 111, A10220, doi:10.1029/2006JA011676.

Niemann, H. B., et al. (2005), The abundances of constituents of Titan's atmosphere from the GCMS instrument on the Huygens probe, *Nature*, *438*, doi:10.1038/nature04122.

Omidi, N., and D. Winske (1987), A kinetic study of Solar wind mass-loading and cometary bow shocks, *J. Geophys. Res.*, *92*, 13,409–13,426.

Porco, C. C., et al. (2005), Imaging of Titan from the Cassini spacecraft, *Nature*, *434*, doi:10.1038/nature03436.

Sillanpää, I., E. Kallio, P. Janhunen, W. Schmidt, K. Mursula, J. Vilppola, and P. Tanskanen (2006), Hybrid simulation study of ion escape at Titan for different orbital positions, *Adv. Space Res.*, *38*, 799–805.

Simon, S., A. Böβwetter, T. Bagdonat, U. Motschmann, and K.-H. Glassmeier (2006), Plasma environment of Titan: A 3-D hybrid simulation study, *Ann. Geophys.*, *24*, 1113–1135.

Sittler, E. C., Jr., R. E. Hartle, A. F. Viñas, R. E. Johnson, H. T. Smith, and I. Mueller-Wodarg (2005), Titan interaction with Saturn's magnetosphere: Voyager 1 results revisited, *J. Geophys. Res.*, *110*, A09302, doi:10.1029/2004JA010759.

Szego, K., et al. (2005), The global plasma environment of Titan as observed by Cassini Plasma Spectrometer during the first two close encounters with Titan, *Geophys. Res. Lett.*, *32*, L20S05, doi:10.1029/2005GL022646.

Waite, J. H., Jr., et al. (2005), Ion neutral mass spectrometer results from the first flyby of Titan, *Science*, *308*, doi:10.1126/science.1110652.

Young, D. T., et al. (2004), Cassini plasma spectrometer investigation, *Space Sci. Rev.*, *114*, doi:10.1007/s11214-004-1406-4.

Young, D. T., et al. (2005), Composition and dynamics of plasma in Saturn's magnetosphere, *Science*, *307*, doi:10.1126/science.1106151.

P. Janhunen, R. Jarvinen, E. Kallio, and I. Sillanpää, Finnish Meteorological Institute, P.O. Box 503, FIN-00101 Helsinki, Finland. (ilkka.sillanpaa@fmi.fi)